heritage

MDPI

Article

The San Saturnino Basilica (Cagliari, Italy): An Up-Close Investigation about the Archaeological Stratigraphy of Mortars from the Roman to the Middle Ages

Fabio Sitzia [1,2]

[1] HERCULES Laboratory, Institute for Advanced Studies and Research, University of Évora, Largo Marquês de Marialva 8, 7000-809 Évora, Portugal; fsitzia@uevora.pt
[2] Geosciences Department, School of Sciences and Technology, University of Évora, Rua Romão Ramalho 59, 7000-671 Évora, Portugal

Abstract: The manufacturing technology of historical mortars from the Roman to Medieval period apparently has not undergone evolutions. As reported in the literature, a quality decrease in the raw material occurred after the fall of the Roman Empire. During the Roman Age, the mortars presented the requirements of long durability due to hydraulic characteristics, and in later times, the production has only partially maintained the ancient requirements. To focus on the different production technologies between Roman and Medieval mortar, this research presents the case study of San Saturnino Basilica (Italy), where an archaeological mortar stratigraphy from Roman to Middle Ages is well preserved. An archaeometric characterization was performed to compare the mortars of the Roman period with the mortars of the Medieval period collected from the case-study monument. This comparison was carried out by measuring some physical-mechanical, mineralogical, petrographic and thermal features that give more information about the durability and resistance to mechanical solicitations and weathering. After the characterizations, contrary to what is reported in the bibliography, a better quality of Medieval materials than Roman ones is pointed out. This has been highlighted by higher hydraulicity, mechanical performance, and a more appropriated particle-size distribution of aggregates.

Keywords: Roman mortars; Medieval mortars; binder; thermal characterization; hydraulicity

Citation: Sitzia, F. The San Saturnino Basilica (Cagliari, Italy): An Up-Close Investigation about the Archaeological Stratigraphy of Mortars from the Roman to the Middle Ages. *Heritage* **2021**, *4*, 1836–1853. https://doi.org/10.3390/heritage4030103

Academic Editor: Ákos Török

Received: 13 July 2021
Accepted: 12 August 2021
Published: 16 August 2021

1. Introduction

In antiquity, the ancient workers had the necessity to produce durable mortars, so-called "hydraulic mortars", capable of remaining hard in high-humidity environments and underwater, too. Because of the absence of specialized technologies, they tested a lot of raw materials, discovering the ones that best fit their needs as fragments of volcanic rocks and volcanic ash (pozzolan), defining them as "pozzolanic mortar". In the absence of natural raw materials, they experimented a mixture with the addition of artificial aggregates (e.g., ceramics rubble, brick rubble, and powder tiles).

The hydraulic mortars such as "pozzolanic" or "brick rubble" typology were already known at the time of the Phoenicians and were perfected by Romans. This technology consisted of the use of pure lime mortars with the absence of impurities, whose hydraulicity was subsequently provided by the use of reactive aggregates (brick rubble, pozzolan, obsidian, rhyolite, and coal) [1].

According to this technique, mortars classifiable as "hydraulic mortars based on air lime" were produced. The hydraulicity of aggregates and their great potential were discovered during the III Cent. BC. Those aggregates made it possible to build bridges, piers, and other works in marine environments [1]. The correct manufacturing and use of mortars started approximately after the publishing of the De Architectura book series, written by Vitruvio Pollione in 15 BC [2], until the western Roman empire fell (476 AD) [3].

The Middle Ages saw a widespread and gradual decline in the quality level of mortars [4,5], and an increasing use of impure sands occurred, followed by the use of pozzolan and brick-rubble becoming obsolete [6]. The use of brick was also abandoned, returning to the use of stone, wood, and beaten earth especially for the walls. Only after XIV Cent. AD, Vitruvius texts were translated and reread, rediscovering the art of ancient architects [7]. During the year 1750 AD, hydraulic lime was discovered, and the mortars technology was revolutionized.

The hydraulic lime mortars had similar characteristics to the lime–pozzolan mixture but without the necessity to pozzolanic materials addition. This, in fact, was not available everywhere.

Nowadays, numerous studies investigate the production technology of Roman mortars [8,9]. The following research focuses on some archaeometric studies by comparing the production technology of mortars manufactured in different historical periods. A case study monument, represented by the Basilica of San Saturnino (Cagliari, Italy), composed of a well-preserved archaeological stratigraphy from late Roman times to Medieval Romanesque, has been examined. The structure offers the chance to investigate materials and construction methods related to different cultures from Roman to Contemporary [10]. The Basilica of S. Saturnino (Figure 1a–c) was located, until the last century, in the near eastern outskirts of Cagliari urban centre which gradually incorporated and kept in a green area (Buffer zone, Figure 1b).

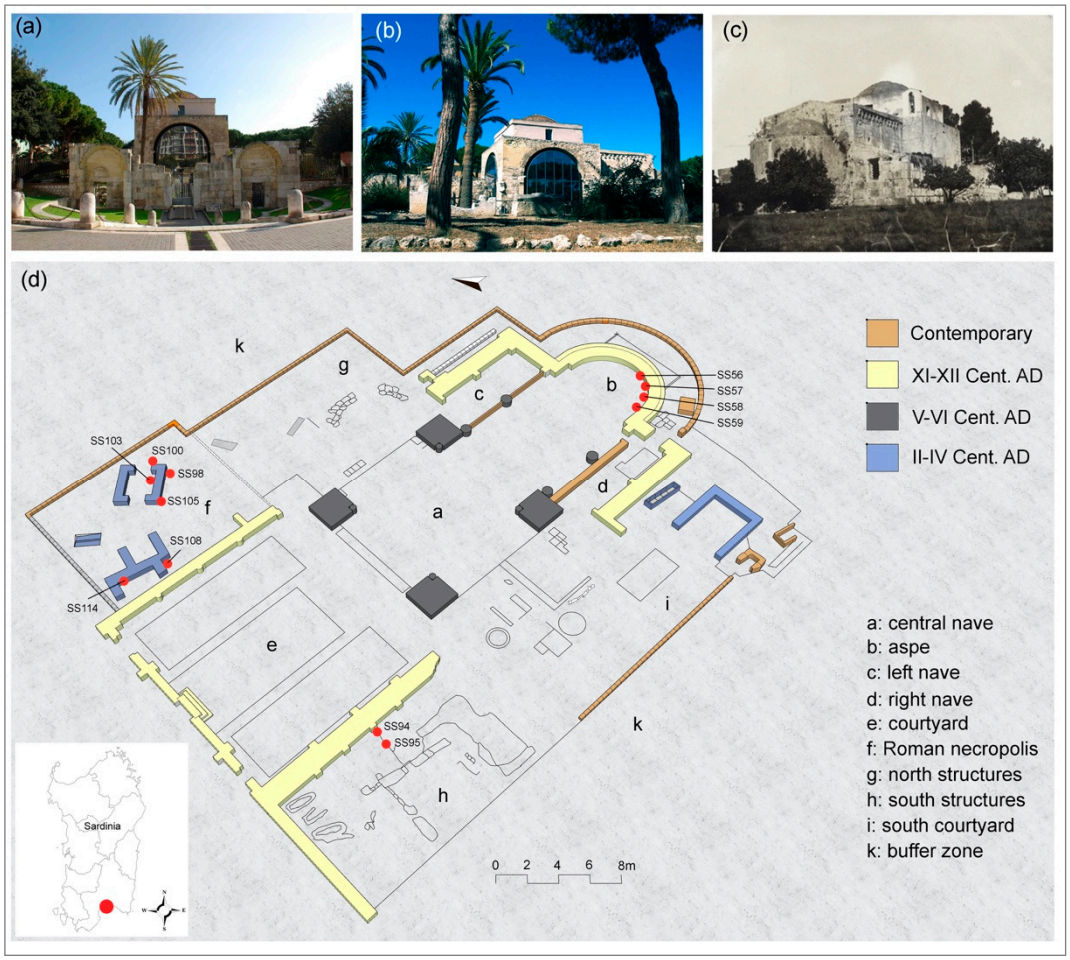

Figure 1. San Saturnino Basilica. (**a**) main facade, (**b**) buffer zone in year 2015, (**c**) the Basilica in years 1905, from www.sardegnadigitallibrary.it/index.php?xsl=2436&id=35635 (accessed on 12 July 2021), Colombini Pio collection, (**d**) sampling points on 3D prospect, digital processing by Fabio Sitzia.

The Basilica area integrates the South Late-Punic structure consisting of large ashlar blocks (III Cent. BC) and a later Roman empire necropolis dates II–IV Cent. AD (North Necropolis) [11].

The first documented mentions of the Basilica came from Fulgentius, bishop of Ruspe [12]. He was exiled in Sardinia together with other African bishops by the vandal King Trasamondo. Fulgentius stayed twice in Cagliari city (post 507-515 AD and 519-523 AD). During this period he founded the Iusta Basilicam Sancti Martyris Saturnini monastery and in August 29, 1087, Pope Victor III exhorted the archbishop of Cagliari and the other islanders bishops to restore the dilapidated churches [13].

In 1089, the monastery was donated by the Cagliari judge Costantino-Salusio II de Lacon-Gunale to the Victorines monks of Marseille, who elected it the seat of the Sardinian priory and restored the Basilica with proto-Romanesque styles, rededicating it in 1119 AD.

In the same years, the Basilica of San Saturnino was ceded by Costantino-Salusio II de Lacon-Gunale, to the abbey of S. Vittore in Marseille. The monks rebuilt and restored the monastery and established the seat of the priory of Cagliari in S. Saturno [14]. The Victorines made an evident reuse of various materials, which at the time were out of context and therefore available for a new implementation. Homogeneous, reused architectural elements were used, probably deriving from a single late Roman or Phoenician building, located nearby [14–16].

At the beginning of our century, a series of restorations works began [17] because of the damage suffered in 1943 air raids [18]. The intervention with the addition of volumes and recent renovations has led to an archaeological stratigraphy consisting of at least four periods (e.g., II–IV, V–VI, XI–XII Cent. AD and Contemporary) [19].

The building materials of the Basilica, such as stones and mostly marbles had already been studied previously. Some researchers showed a mainly provenience from Carrara (North Italy) and from southern Greece [20]. To understand the production technology alongside a millennium, mortars belonging to the later Roman empire (II–IV Cent. AD) and Medieval (Romanesque) period (XI–XII Cent. AD) were analysed and investigated. The comparison study between mortars from different historic periods have already been performed in other Roman constructions by remarking an overall different composition of the aggregates and identifying as one limestone source area was used in different historic periods [21,22]. In other studies, a comparison between Roman, proto-Byzantine and Medieval mortars pointed out the lower quality mortars belonged to the Medieval period [23]. In this research, information about the technology of mixing, packaging, implementation, selection of raw materials, and hydraulicity degree was obtained. In order to study the aforementioned aims, a series of archaeometric analyses already adopted in the literature [24,25] as petrographic observation, particle-size distribution of aggregate, and physical features of the materials have been performed. In addition, mineralogic characterization and thermal tests on binder allow one to understand the degree of mortars hydraulicity [26,27]. The main goal is to understand if the Medieval mortars show the tendency to quality-worsening as already pointed out in the literature.

2. Materials and Methods

2.1. Materials

To investigate about the properties of mortars of historic periods, six samples of later Roman mortars and six samples of Middle-Age (Romanesque) mortars were collected in the Basilica. Samples consist of four ashlar bedding and two curtain wall filling. Ashlar bedding mortars were used in the construction of masonry. They connected and held together other building materials (e.g., bricks, stone, and ashlars) by tenaciously adhering and giving a monolithic structure after hardening. The main function of the bedding mortar is to distribute the load of the overlying parts over the entire horizontal section of the wall, compensating for the roughness of the supporting surfaces of the blocks, in particular the irregular ones of the stone.

The name Curtain filling mortar derives from the technical terminology of a curtain wall. It was a thick wall where two rows of bricks were arranged in parallel way with tens centimetres distance one to the other. These rows, also called curtains, had the function of formwork, and their interspace was filled with a cast of mortar.

The selection of materials during sampling was made by trying to collect a similar number of mortars for both clusters using a hammer and chisel according to the UNI EN 16085 normative (Conservation of Cultural property—methodology for sampling from materials of cultural property, General rules). The selection of the samples was carried out in conformity with the archaeological stratigraphy, collecting cohered mortars to have fragments of suitable size for thin-sections production.

The sampling points and the sample amounts were previously selected according to the local archaeological authorities based on the planimetry represented in Figure 1d. The elevation in cm respect than the main floor was registered to have a tridimensionality about the sampling operation.

2.2. Methods

Petrographic determinations (OM) were carried out by optical polarized microscope Leitz Wetzlar on 30 µm thin sections. Modal analysis of aggregates was determined with points counter on about 300 points for each thin section. Circularity of aggregates was estimated by synoptic table [28].

For pXRD analyses, a Bruker AXS D8 Discovery XRD with a CuKα source, operating at 40 kV and 40 mA, and a Lynxeye 1-dimensional detector was used. Scans were performed from 3 to 75°2θ, with 0.05°2θ step and 1 s/step measuring time by point. Diffract-Eva software from Bruker with PDF-2 mineralogical database (International Centre for Diffraction Data-ICDD) was utilized to interpret the scans.

SEM electron microscopy investigations were performed using a SEM-EDS Hitachi 3700n VP with Bruker Xflash 5010 detector.

Thermogravimetry on the binder (TGA) was carried out using a balance Perkin Elmer model TGA7. The measurements were performed under Ar flow (60 mL/min). Samples were placed in platinum crucibles and scanned in the temperature range from 30 to 850 °C with heating rate of 10 °C/min.

Differential scanning calorimetry (DSC) tests on binder were performed at constant atmospheric pressure using a Perkin Elmer DSC7. The tests are carried out with Ar flow (60 mL/min) on 5 mg sample placed in Platinum crucibles. The scanning temperature consists of a range of 30–650 °C with a heating rate of 10 °C/min. The DSC7 instrument was calibrated by measuring the melting temperature of the metallic indium and zinc (99.999% purity), and the temperature was obtained with an accuracy of $\pm$0.5 °C.

Before thermal analysis, the binders were manually separated to the aggregate by a stereo-microscope Wild Heerbrugg.

The binder/aggregate ratios of the mortars were determined by acid dissolution of binder fraction (with HCl 13% concentrated solution) for 48 h immersion. The particle-size distribution (PSD) of residual aggregate was obtained using sieves with mesh openings of 8000, 4000, 2000, 1000, 500, 250, 125, and 63 µm, according to UNI 3121 series.

Real density, imbibition coefficient and water open porosity were performed on 15 mm $\times$ 15 mm $\times$ 15 mm $\pm$ 2 mm specimens according to the methods used to some authors [8] by using a Sartorius CPA324S balance and Quantachrome ULTRAPY1200e Pycnometer.

Real density and water open porosity measurements were conducted according to UNI EN 1936:2007 standard

(Natural stone test methods—determination of real density and apparent density, and of total and open porosity).

Imbibition coefficients were measured according to standard UNI EN 14617-1:2013 (Agglomerated stone—Test methods—Part 1: Determination of apparent density and water absorption)

Point load index (Is_{50}) was determined by point load tester (Controls instrument D550). The compressive strength (R_C) and the tensile strength (R_T) were indirectly calculated from point load strength index according to Palmstrom (1995) [29].

3. Results and Discussions

3.1. Macroscopic Observations, Optical Mineralogy, and SEM-EDS Observations

The mortars of San Saturnino Basilica show a macroscopic colour from light grey (CIELAB 85∗1∗2) to dark grey (CIELAB 51∗2∗3). All the samples display a conglomeratic and microconglomeratic structure.

The binder has rare lumps of lime up to 4 mm in size, in percentages from 1 to 7% volume. The cohesion is moderate.

The optical observation on the thin section pointed out, in both Roman and Romanesque mortars, a poorly welded binder with some shrinkage fractures of 250 µm width and irregular spacing. Binder presents hydrated overcooked lumps (Figure 2a) and agglomerates according to the classification of lime lumps adopted by Pecchioni et al. (2018) [30]. The presence of this type of lumps indicates a not uniform temperature in the lime kiln and insufficient mixing of the dough. As reported in Table 1, in both groups, the aggregate is composed of rock rubble (0–5.8%), bioclasts (0–3.9%), sialic (91.7–99.8%), and femic crystal-clasts (0–0.5%).

Table 1. Modal percentage analysis of mortar aggregates.

Mortar Age	Sample	Function	Rock Rubble	Bioclasts	Sialic Crystal-Clasts	Femic Crystal-Clasts
			(%)	(%)	(%)	(%)
Romanesque (XI–XII Cent. AD)	SS 56	Ashlar bedding	2.3	0.5	97.2	0.0
	SS 57	Ashlar bedding	4.8	1.2	94.0	0.0
	SS 58	Ashlar bedding	4.3	1.0	94.7	0.0
	SS 59	Ashlar bedding	2.1	1.4	96.5	0.0
	SS 94	Curtain wall filling	0.0	0.0	99.8	0.2
	SS 95	Curtain wall filling	0.0	0.3	99.7	0.0
Roman (II–IV Cent. AD)	SS 100	Ashlar bedding	5.2	1.6	93.2	0.0
	SS 103	Ashlar bedding	5.8	1.3	92.9	0.0
	SS 105	Ashlar bedding	3.9	3.9	91.7	0.5
	SS 114	Ashlar bedding	1.0	3.1	95.9	0.0
	SS 108	Curtain wall filling	3.5	1.0	95.5	0.0
	SS 98	Curtain wall filling	3.6	1.8	94.1	0.5

Rock rubble is mainly represented by sandstone fragments (Figure 2b,g,h), with variable clay amount, dimensions ranging from submillimetre to centimetre and circularity degree C > 0.5. The rock rubble secondly consists of limestones and pebbles with (C > 0.5).

In all the thin sections of Roman and Romanesque mortars, the fossiliferous components, when present, point out bioclasts of foraminifera (Figure 2f), gastropods, bivalves and coralline algae.

The crystal-clasts (Figure 2e) are mainly represented by quartz, high-altered feldspar, clinopyroxene, biotite, and opaques. All the clasts have a circularity degree C > 0.5.

The high circularity of crystal-clasts and a fossiliferous fauna of marine environment suggest the probable use of marine sand as aggregate. It could be probably extracted from the current Giorgino and/or Poetto beaches located some kilometres south. From Roman to Middle Ages to contemporary periods, in these beaches, the sampling of sand continued until the period 1943–1989 used for civil building construction at Cagliari and Quartu cities [31].

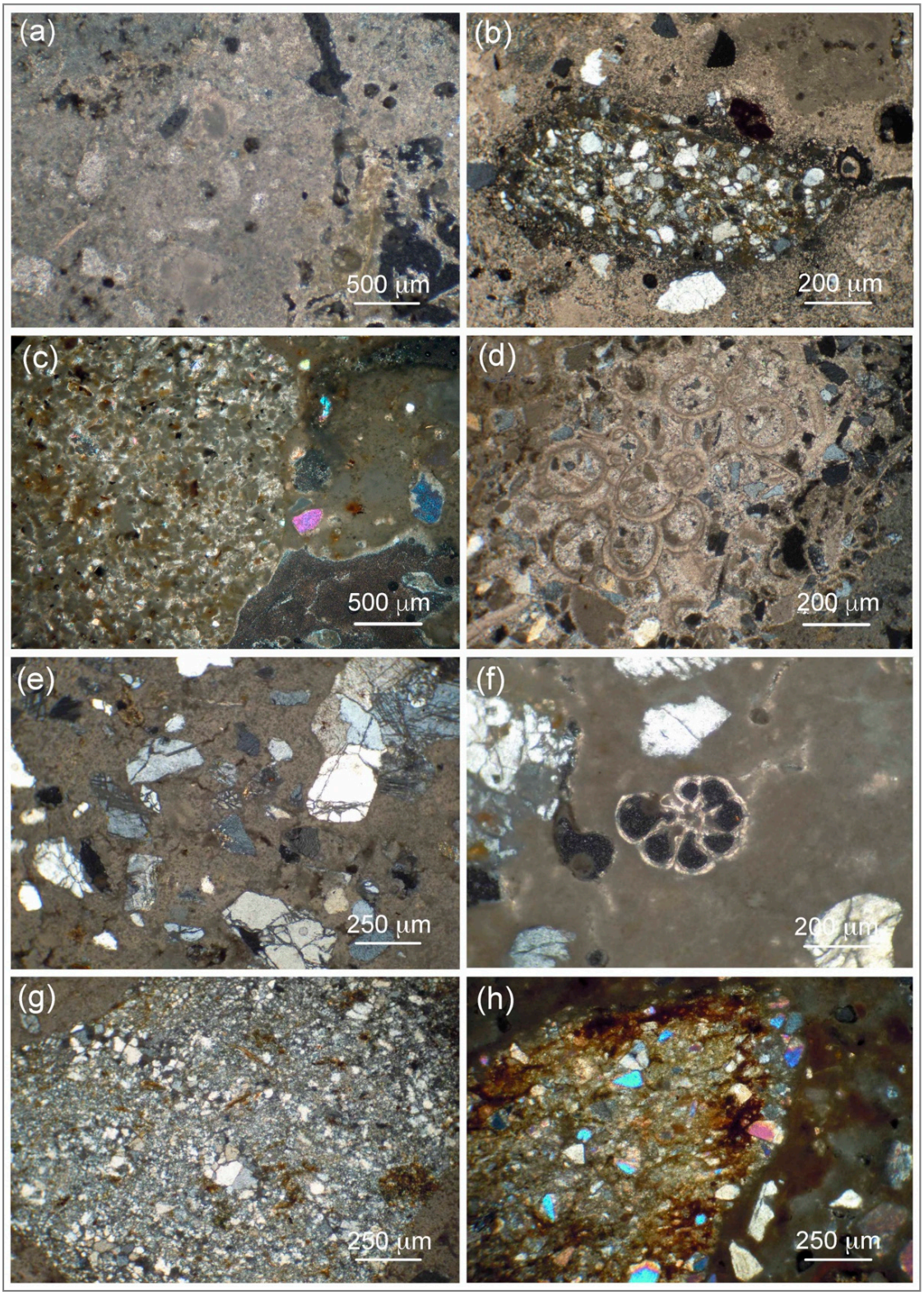

Figure 2. OM observation on San Saturnino mortars. (**a**) Binder lump on ashlar bedding mortar SS105, (**b**) sandstone fragment with quartz clasts and clay content on ashlar bedding mortar SS100, (**c**) "ghost" that preserves the original structure of biomicrite raw material (ashlar bedding mortar SS103), (**d**) "ghost" that preserves the original structure of biolitite raw material on ashlar bedding mortar SS114, (**e**) quartz crystal-clasts of quartz and K-feldspar on SS59, (**f**) umbilica cross section of foraminifera bioclast (probably planktonic *Neogloboquadrina*) on SS58, and (**g**,**h**) rock rubble aggregates sandstone (pebbles) on the sample SS57.

In the 1990s, at Poetto, the volumetric depletion of the beach was significant because the sand collected for building purpose was no longer compensated by the sedimentary contributions from the hinterland. This led to a beach nourishment intervention in early 2000s.

Normally, during Roman times, the sea sand was carefully washed with fresh water to remove impurity and sodium chloride. This was also recommended by the Architect Vitruvio in 15 BC. Sodium chloride could alter the setting times of the mortar itself and cause other decay due, for example, to the following chemical reaction, which forms high-soluble compounds products as in reaction (1) and reaction (2).

$$2NaCl\ (\text{sodium chloride}) + CaCO_3\ (\text{calcium carbonate}) \rightarrow Na_2CO_3\ (\text{sodium carbonate}) + CaCl_2\ (\text{calcium chloride}) \quad (1)$$

$$\text{C-A-H (hydraulic gel)} + NaCl\ (\text{sodium chloride}) \rightarrow Ca_4Al_2(OH)_{12}(Cl,CO_3,OH)_2 \cdot 4H_2O\ (\text{Hydrocalumite}) \quad (2)$$

Although the Roman and Romanesque mortars were produced at a distance of about a millennium, the observation in thin section allowed one to fairly identify similar mineralogy and percentage of the aggregates on the basis of the function adopted in the building.

Some calcareous fragments ("ghosts") that preserve the original structure of the raw limestone material due to inadequate firing in the kiln have been found (Figure 2c,d) on Romanesque mortars. These fragments have been recognized as local biomicrites and biolitites. These stones were also employed for realizing the Basilica ashlars [32,33].

According to the literature, this calcareous material came from nearest quarries located on Bonaria Hill, 700 m in the southeast direction. Inside the quarries, the ancient traces of extraction are compromised by the excavations in later times as well as the widespread presence of debris.

The biomicrite (locally called Pietra Cantone) is a impure limestone with 5–15% vol. of clay (e.g., illite and kaolinite), considered capable of giving weak hydraulic properties to the mortar [34]. The use of biomicrites, started during Roman Republican age, continued until the 1960s at metropolitan area of Cagliari for cement production [35].

The biolitite (locally called Pietra Forte) does not present particular hydraulicity properties because of its ≈100% calcite paragenesis.

The use of biomicrites and biolitites for binders production can be testified by the discovery in a Romanesque sample of a floor concrete consisting of two different binders placed in contact. The two binders macroscopically differ in colour (brownish CIELAB 62∗−2∗49 for binder 1 vs. whitish CIELAB 82∗2∗3 for binder 2). The different colours also are well visible on thin section (Figure 3).

A SEM-EDS point measurement on the two binders shows a different chemical composition (Figure 3). Binder 1 has calcium and oxygen contents Ca = 40.44 Wt.%, and O = 47.71 Wt.% and relatively low levels of Si = 2.48 Wt.%, Al = 0.13 Wt.%, and C = 8.26 Wt.%.

Binder 2 has calcium and oxygen contents Ca = 11.53 Wt.%, O = 30.69 Wt.%, Si = 24.70 Wt.%, Al = 2.86 Wt.%, and C = 26.57 Wt.%. The analysis shows a higher Silicon and Aluminium content on binder 2.

As we can see in Section 3.3, different hydraulic properties of San Saturnino mortars, have been identified in TGA analysis. It cannot be excluded that the different composition of the two binders derives from the use of limestone facies with different clay content to produce mortars, such as biomicrite and biolitite. It is not possible to understand which type of intervention involved the use of the two binders in contact; however, it could be a probable restoration intervention or a new cast lying. It is also probably that the two binders present different age, but this is only a hypothesis that can be confirmed in further studies.

Mortars of both cultures do not present pozzolanic aggregates, even if in other Roman buildings, materials such as brick rubble and obsidian have been found [36].

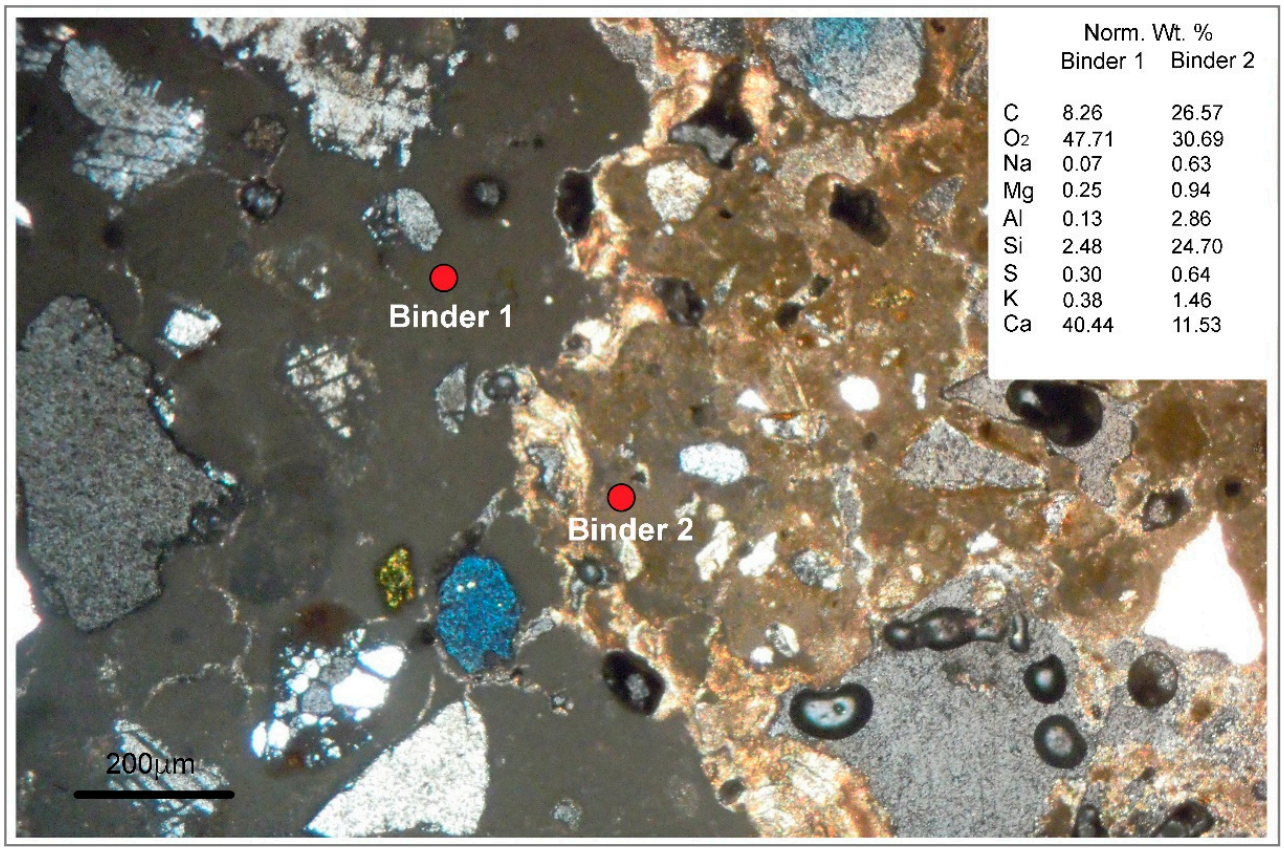

Figure 3. Thin-section photo with SEM-EDS point analysis on the binder 1 and binder 2. Binder 1 on the left presents a macroscopic colour as brownish (CIELAB 62∗−2∗49); Binder 2 on the right has a whitish CIELAB 82∗2∗3 macroscopic colour. A chemical composition with C, O_2, Na, Mg, Al, Si, S, K, and Ca is available on the title block.

As identified in thin section, some pozzolanic reaction rims have been identified on the interface pebble-binder. The Figure 4 exhibits a portion of thin section in secondary electrons (Figure 4a) and OM (Figure 4b) where some aggregate clasts show some pozzolanic rims.

Two line scans (a, b) have been performed in order to investigate the trend of the elements Ca, Al, Si, O, and C composing the hydraulic gel C-A/S-H on the reaction rims. The elements present a similar trend into the two scan lines, indicating the presence of a binder-aggregate chemical rim located between 48–55 point number on line a and 77–82 on line b (Figure 4). Here, the elements Ca, Al, and Si have an intermediate concentration with respect to the nucleus of the clast and the binder. The variation trend of the chemical elements in the reaction rims is similar to those described by Moropoulou et al. (2000) [26] and Crisci (2004) [27] on fragments of brick rubble and pozzolan. In the reaction rims, a low value of Al and Si respect than the aggregate core and a high value of Ca are due to the increase in volatiles in the neoformation hydraulic phases [37].

3.2. pXRD Diffraction on Binder

X-ray diffraction on San Saturnino binders (Table 2) was useful for identifying secondary alteration mineral phases and accessory not observable by OM. The Roman mortars consist of calcite and quartz-feldspathic phases. These phases could be found in the binder due to an incomplete manual separation of the aggregate.

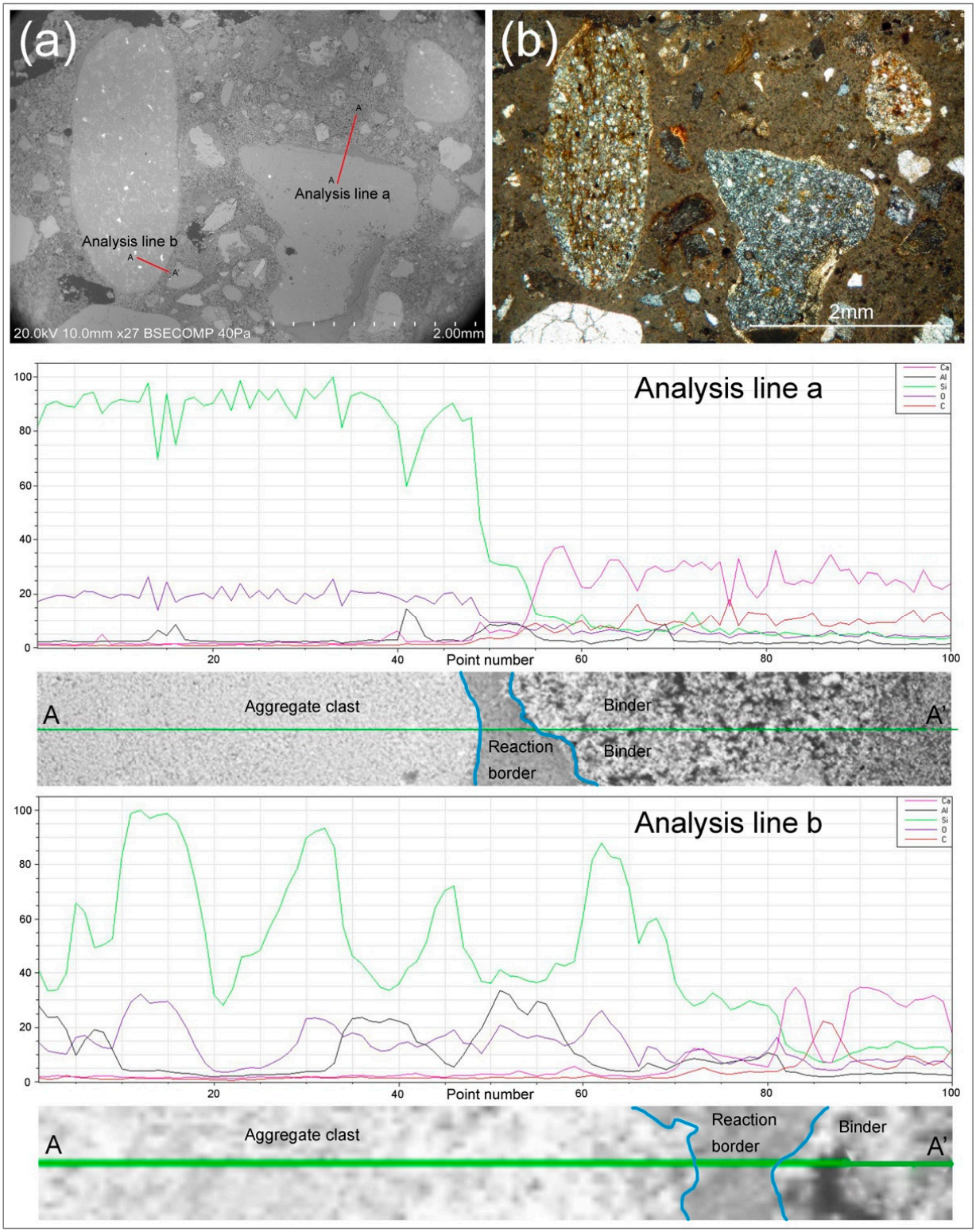

Figure 4. SEM-EDS analysis: (**a**) SEM secondary electron photo of two pebble aggregates with reaction border. The line scans a and b crossing the reaction border are indicate in green. (**b**) OM photo of two pebble aggregates with reaction rim. The lower part of the photo indicates the trends of the elements Ca, Al, Si, O, and C from aggregates clasts core to the binder. The concentration of the chemical elements Ca, Al, and Si in the reaction border is an intermediate between binder and aggregate clast. In addition, the presence of a low value of Al and Si respect than the aggregate core and a high value of Ca is due to the increase in volatiles in the neoformation hydraulic phases.

Table 2. (pXRD) diffraction on San Saturnino mortars: Ca = calcite, Qz = quartz, Pla = plagioclase, Kf = K-feldspar, Bio = biotite, Gy = gypsum, Kao = kaolinite, Hal = halite, Vat = vaterite, Ara = aragonite, Kz = kuzelite, Msp = monosulphate, Alu = aluminite. Tr = traces (≤2% wt.), "●" indicates present (2–10% wt.), "●●" indicates abundant (10–40% wt.) and "●●●" indicates very abundant (≥40% wt.).

Sample	Mortar Age	Function	Ca	Qz	Pla	Kf	Bio	Gy	Kao	Hal	Vat	Ara	Kz	Msp	Alu
SS 56	Romanesque XI–XII Cent. AD)	Ashlar bedding	●●	●●	●	●●	●	-	●	-	-	-	-	-	-
SS 57		Ashlar bedding	●●	●●	●●	●	●	-	Tr	-	-	-	-	-	-
SS 58		Ashlar bedding	●●	●●●	●	●●	●	Tr	Tr	-	-	-	-	-	-
SS 59		Ashlar bedding	●●	●●	●	●	●	-	Tr	-	-	-	-	-	-
SS 94		Curtain wall filling	●●	●●	●●	●●	●	-	Tr	-	-	-	-	-	-
SS 95		Curtain wall filling	●●	●	●●	●●	●	-	Tr	-	-	-	-	-	-
SS 100	Roman (II–IV Cent. AD)	Ashlar bedding	●●	●●	●●	●●	●	Tr	-	-	-	-	Tr	-	-
SS 103		Ashlar bedding	●●	●●	●	●	●	-	-	Tr	-	-	-	-	-
SS 105		Ashlar bedding	●●	●●	●	●	●	Tr	●	-	Tr	-	-	-	-
SS 114		Ashlar bedding	●●●	●	-	●●	Tr	●	-	-	-	●	-	-	●
SS 98		Curtain wall filling	●●	●●	●●	●	●	-	Tr	-	-	Tr	-	Tr	-
SS 108		Curtain wall filling	●●	●●	●	●	●	-	-	-	-	-	-	-	-

In addition to calcite, the polymorph of calcium carbonate vaterite was detected in traces on SS105 (Table 2). The aragonite, another polymorph of calcium carbonate, was detected on SS114 and SS98 (Table 2). The presence of vaterite and aragonite in historical and contemporary cements and mortars is well documented and it is attributable to bioclasts. In SS105, SS114 and SS98, the presence of bioclasts from 1.8 to 3.9% is confirmed by OM observations (Table 1). The formation of the two $CaCO_3$ polymorphs is also due to the carbonation temperature of the portlandite $Ca(OH)_2$ [38,39]. Calcite and vaterite are both low temperature polymorphs (30 °C) but already at 40 °C vaterite becomes predominant. Aragonite is also formed at 40 °C and becomes predominant at 60–80 °C [40,41]. In any case, at any temperature and over time, the two polymorphs of $CaCO_3$ still tend to transform into more stable calcite. In Roman mortars, gypsum has been identified as a sulphation product of calcium carbonate, probably due to anthropic sulphate anion or from marine aerosols (*ESA*, *External Sulphate Attack*) [42]. In confirmation of this second hypothesis, measurements by meteorologic satellite (data from the GIOVANNI meteorological portal, National Aeronautics and Space Administration), show in San Saturnino area an atmospheric concentration of marine spray relatively high (3.26×10^{-8} < MSpray < 3.61×10^{-8} Kg/m^3). Monthly marine spray deposition on buildings is not available but can be considered high due to an average monthly wind speed of 15 Km/h (Data Portal AM, Italian Air Force). The presence of marine spray in atmospheric suspension is also confirmed by traces of halite (NaCl) on SS103 (Table 3).

Table 3. Thermal characterization (TGA) on binders (italic differentiates standard deviations and arithmetic averages from the rest of the data).

Sample	Mortars Age	Function	Weight Lost in Temperature Ranges (%)		$\Delta CO_2/\Delta H_2O$
			200–520 °C (ΔH_2O)	520–800 °C (ΔCO_2)	
SS 56	Romanesque (XI–XII Cent. AD)	Ashlar bedding	5.08	11.12	2.19
SS 57		Ashlar bedding	4.02	10.80	2.69
SS 58		Ashlar bedding	2.61	15.36	5.89
SS 59		Ashlar bedding	2.80	11.62	4.15
SS 94		Curtain wall filling	2.09	25.34	12.12
SS 95		Curtain wall filling	2.90	19.17	6.61
	Arithmetic average		*3.25*	*15.57*	*5.61*
	Standard deviation		*1.10*	*5.77*	*3.63*
SS 100	Roman (II–IV Cent. AD)	Ashlar bedding	3.36	24.26	7.22
SS 103		Ashlar bedding	2.27	28.18	12.41
SS 105		Ashlar bedding	2.64	22.16	8.39
SS 114		Ashlar bedding	2.71	25.08	9.25
SS 108		Curtain wall filling	6.13	19.75	3.22
SS 98		Curtain wall filling	2.92	25.06	8.58
	Arithmetic average		*3.34*	*24.08*	*8.18*
	Standard deviation		*1.41*	*2.87*	*2.99*

In Roman mortars, traces of calcium and aluminium hydrated sulphates (kuzelite, $Ca_4Al_2(SO_4)(OH)_{12}\cdot 6H_2O$) were found as hydration product of ettringite [43]. The formation of this last compound is expressed in the following chemical reactions:

$$SO_4^{-2} + Ca(OH)_2 \text{ (portlandite)} \rightarrow CaSO_4\cdot 2H_2O \text{ (gypsum)} + 2OH \quad (3)$$

$$CaSO_4\cdot 2H_2O \text{ (gypsum)} + \text{C-A-H (hydrated calcium aluminates)} \rightarrow Ca_6Al_2(SO_4)_3(OH)_{12}\cdot 26H_2O \text{ (ettringite)} \quad (4)$$

The ettringite formation begins with the sulphate anion reacting with mortar portlandite to generate gypsum reaction (3). Subsequently, the latter reacts with the hydrated calcium aluminates (C-A-H) according to reaction (4).

Other calcium and aluminium sulphates such as aluminite $Al_2(SO_4)(OH)_4 \cdot 7H_2O$ and monosulphate $Ca_4Al_2O_6(SO_4) \cdot 14H_2O$ were found on SS114 and SS98 (Table 3). They derive from a process subsequent to the formation of ettringite, where the sulphate anion during the reaction (3) begins to run out, by producing poorer sulphur compounds in reaction (4) [43].

In Romanesque mortars, a simple mineralogical composition represented by calcite and prevailing sialic phases was detected (Table 3). Traces of gypsum were also detected on SS58, which probably represents a sulphation product of the carbonate binder. Kaolinite is present in all Romanesque mortar samples and probably derives from the hydrolysis of plagioclases and K-feldspars, a process already observed in thin section on the crystal-clasts. Part of the kaolinite could also come from "ghost" fragments of biomicritic stone that, as mentioned above, has a certain content of syngenetic clay minerals.

3.3. Thermal TGA and DSC Analysis on Binder

The curves obtained in simultaneous TGA/DSC analysis on the binders of Romanesque and Roman mortars evidence some characteristic weight losses (Figure 5a,b).

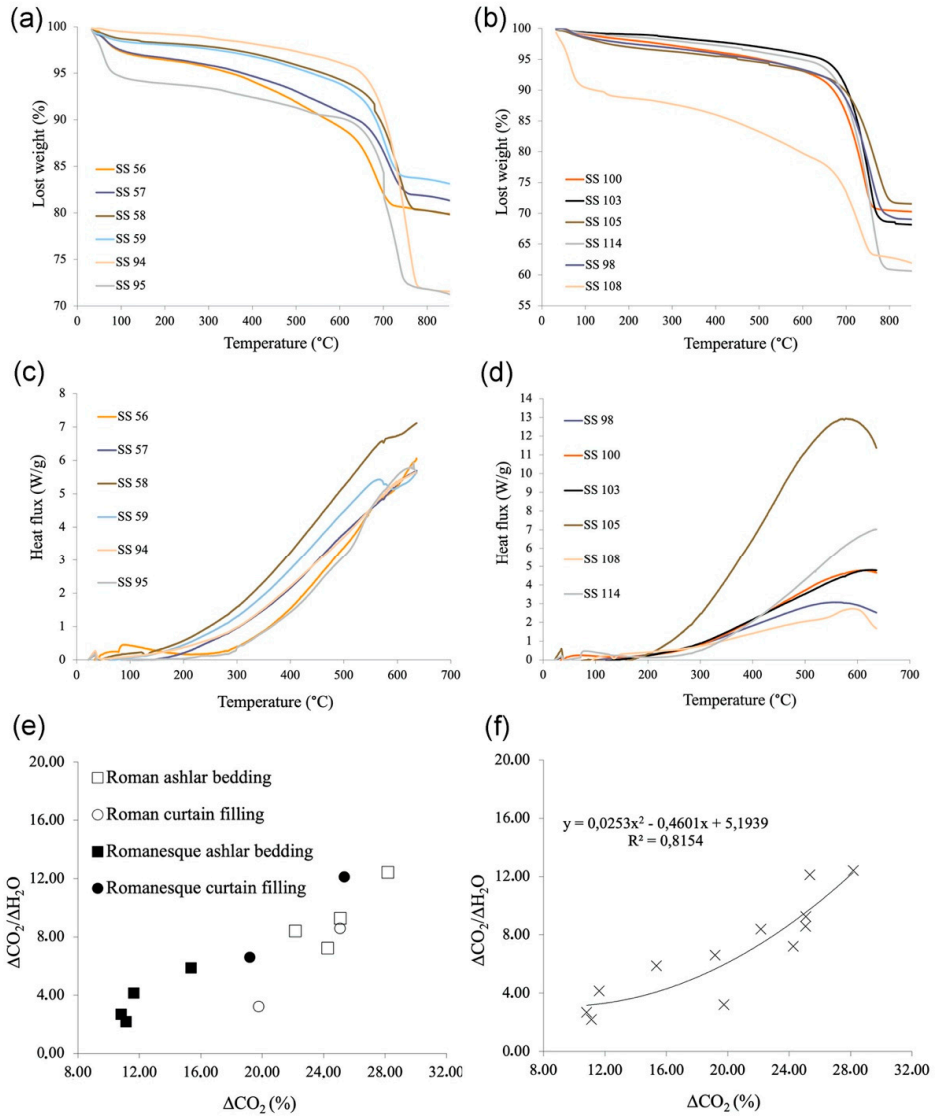

Figure 5. Thermal analysis: (**a**) thermal decomposition curves of Romanesque mortars, (**b**) thermal decomposition curves of Roman mortars, (**c**) differential scanning calorimetry on Romanesque mortars, (**d**) differential scanning calorimetry on Roman mortars, (**e**) ΔCO_2 vs. $\Delta CO_2/\Delta H_2O$ diagram for Romanesque and Roman mortars, and (**f**) ΔCO_2 vs. $\Delta CO_2/\Delta H_2O$ diagram for all the samples.

The initial trend of the thermal decomposition curves has a weight loss at 30–50 °C due to the evaporation of capillary water (humidity), confirmed by the endothermic thermodynamics of the reaction detectable in the corresponding DSC curves (Figure 5c,d).

A further weight loss is detected in some samples such as SS58, SS100, SS101, SS102, and SS114, and it is due to the dehydration process of the gypsum already detected in diffraction (Table 2). At temperatures of about 100 °C the dehydration of gypsum occurs, eliminating part of the water (about 75% vol.) present in the chemical structure by producing anhydrite. This process can take place in a range from 90 to 130 °C, according to the degree of crystallinity of the phase.

A pozzolanic weight loss is detectable only in some samples (SS105, SS114) usually localized in a temperature range between 480 and 550 °C associated with the loss of carbon dioxide [44] according to the following reaction:

$$CaCO_3 \text{ (calcite)} + XSiO_2 \text{ (silicates)} \rightarrow CaXSiO_3 \text{ (calcium silicates)} + CO_2 \text{ (X = K, Al, F)} \quad (5)$$

Calcite and silicates present in the binder react to form calcium silicates and carbon dioxide. This reaction is identified in the diagrams of Figure 5c,d as a negative peak associated with an endothermic thermodynamics.

The most extensive weight loss is found in a temperature range between 520 and 800 °C related to the decarbonation of the calcitic binder.

The weight loss linked to the decarbonation is slightly accentuated in the samples, as a result of a discrete compositional heterogeneity of the binders. Small losses in weight between 550 and 600 °C of endothermic thermodynamics are visible in the sample SS57 and SS95 and could be attributed to the dehydration process of the kaolinite with the formation of metakaolinite [45] (4):

$$Al_2Si_2O_5(OH)_4 + \text{Heat} \rightarrow Al_2Si_2O_7 \text{ (metakaolinite)} + 2H_2O \quad (6)$$

In Figure 5f, the samples of Romanesque and Roman mortars combined in a single series present a polynomial correlation line with R^2 = 0,81. By observing the Figure 5e and the Table 3, we note an average higher hydraulicity in the binders of Romanesque mortars than in Roman ones (ΔCO_2 = 15.57 vs. 24.08% respectively). This difference could be due to the use of two raw materials giving a different hydraulicity as biomicrite and biolitite. Even within the same group, differences in hydraulicity between samples could be explained in the same way. Assuming a single extraction area, the alternative use of biomicrite and biolitite would have resulted from a geological contact present in the quarry. It is also possible to hypothesize that, in order to avoid the process of sawing and transporting of the rock, erratic blocks of biomicrite and biolitite rotated downstream from the top of the hills were used. This practice had already been performed in the construction of other monuments [46].

3.4. Particle-Size Distribution of the Aggregates

The particle-size distribution of San Saturnino mortars are shown in Tables 4 and 5. The B/A ratios are strictly connected to the function that the mortars have in the structure.

The Romanesque ashlar bedding mortars have a B/A ratio 0.30 < B/A < 0.53 with an average of 0.37. The curtain fillings present B/A ratio of 0.83 and 0.92 with an average of 0.87.

In the Roman ashlar bedding mortars, 0.23 < B/A < 0.38 with an average of 0.29. Romanesque curtain filling presents a B/A ratio of 0.88 and 0.90, with an average of 0.89.

From these data, it is possible to understand how between Roman and Romanesque mortars, the mixing ratios are rather similar both for bedding mortars and curtain fillings. It is likely that in the Medieval period there was the intention to replicate a binder/aggregate mixture similar to the Roman mortars already present in situ known for their durability.

The PSD (Table 4) show how all the Romanesque ashlar bedding mortars are very similar and represented by 2000–1000 μm aggregates (very coarse sand) [47].

Table 4. Particle-size distribution (PSD) of mortar aggregates: hold mass percentage according to UNI 3121 sieve series, B/A = binder/aggregate ratio.

Sample	Mortar Age	Function	B/A	Hold Mass (%)								
				8000 μm	4000 μm	2000 μm	1000 μm	500 μm	250 μm	125 μm	63 μm	<63 μm
SS 56	Romanesque (XI–XII Cent. AD)	Ashlar bedding	0.30	0.00	3.93	22.48	36.51	18.66	9.09	7.85	1.42	0.07
SS 57		Ashlar bedding	0.33	5.32	7.60	24.41	32.78	14.73	8.02	5.97	1.08	0.08
SS 58		Ashlar bedding	0.53	6.42	5.15	18.82	29.31	15.60	11.77	9.31	2.71	0.90
SS 59		Ashlar bedding	0.33	0.00	8.11	21.47	31.86	17.60	9.00	8.68	2.35	0.92
SS 94		Curtain wall filling	0.92	0.00	6.61	21.75	16.32	7.46	26.60	17.09	3.72	0.46
SS 95		Curtain wall filling	0.83	0.00	1.49	13.40	15.30	14.39	41.57	13.71	0.13	0.00
SS 100	Roman (II–IV Cent. AD)	Ashlar bedding	0.23	0.00	9.09	20.79	25.38	18.11	17.81	6.98	1.71	0.13
SS 103		Ashlar bedding	0.30	2.37	4.47	8.64	23.22	27.64	31.09	2.57	0.00	0.00
SS 105		Ashlar bedding	0.27	2.51	25.73	29.57	13.11	11.16	9.73	4.95	3.21	0.04
SS 114		Ashlar bedding	0.38	0.00	3.86	33.28	21.48	10.39	16.18	11.82	2.82	0.17
SS 98		Curtain wall filling	0.90	0.00	2.50	8.01	17.93	19.54	33.20	11.53	4.04	3.25
SS 108		Curtain wall filling	0.88	0.00	2.28	10.09	34.33	20.63	18.86	9.00	4.10	0.71

Table 5. Particle-size distribution (PSD) of mortar aggregates: midpoint passing diameters on 60–10% and coefficients of uniformity.

Sample	Mortar Age	Function	Midpoint Passing Diameter on 60% D_{60} (μm)	Midpoint Passing Diameter on 10% D_{10} (μm)	Niformity Coefficient U = D_{60}/D_{10}
SS 56	Romanesque (XI–XII Cent. AD)	Ashlar bedding	1500	280	5.35 (various)
SS 57		Ashlar bedding	1900	350	5.42 (various)
SS 58		Ashlar bedding	1200	210	5.71 (various)
SS 59		Ashlar bedding	1500	220	6.81 (various)
SS 94		Curtain wall filling	1100	175	6.28 (various)
SS 95		Curtain wall filling	580	230	2.52 (uniform)
SS 100	Roman (II–IV Cent. AD)	Ashlar bedding	1450	270	5.37 (various)
SS 103		Ashlar bedding	1000	300	3.33 (uniform)
SS 105		Ashlar bedding	3000	300	10 (various)
SS 114		Ashlar bedding	1900	200	9.5 (various)
SS 98		Curtain wall filling	640	170	3.76 (uniform)
SS 108		Curtain wall filling	990	200	4.95 (uniform)

On SS94, a bimodal PSD has mainly 2000 and secondly 250 μm hold masses. The sample SS95 points out a fine aggregate represented by mainly 250 and secondly 500 μm (medium sand).

The Roman mortars have more differentiated PSD as 2000–1000 μm (very coarse sand on SS100, SS114) and 500–250 μm (medium sand on SS103, SS98). On SS105, a PSD represented by granules (4000–2000 μm) has been detected. Table 5 exhibits how all the Romanesque mortars have a various PSD except for sample SS95.

In Roman mortars 50% of the samples present a uniform particle size and the other 50% various.

Vitruvius' recommendations that advise a various PSD to save binder and improve the mechanical performance of the mortar seem to be more respected in Medieval mortars.

3.5. Physical-Mechanical Analysis

Physical analysis reported in Table 6 underline higher densities in Romanesque mortars in respect to Romans. An imbibition coefficient of 18.82 ± 4.85% vs. 20.58 ± 3.12% is measured in Romanesque and Roman mortars, respectively. One of the most important parameters, the total porosity, is lower in Romanesque mortars with a value of 41.07 ± 6.08%. This amount of total porosity consists of 34.44 ± 5.03% of Helium open porosity and 6.63 ± 2.20% of closed porosity. In Roman mortars, similar percentages are recorded with Φ_t = 43.13 ± 4.02%, where ΦHe = 36.77 ± 3.21% and Φ_c = 6.36 ± 1.89%. The saturation index is similar in the two groups with S.I. = 91.08 ± 5.23% vs. 89.66 ± 2.77% for Romanesque and Roman mortars respectively. The property that well discriminate the two groups is the point load strength index. Is_{50} = 0.77 ± 0.17% in Romanesque mortars and Is_{50} = 0.66 ± 0.13% in Roman mortars were detected (Table 7). This difference of mechanical resistance is also reflected in compression and tensile strengths. The higher resistance in Romanesque mortars could be explained with lower porosity, a various PSD and different raw materials used for binder, as also confirmed by higher hydraulicity of this group.

Table 6. Physical analysis of mortars. ρ_R = real density, ρ_B = apparent density, ρ_S = solid density, CI_W = imbibition coefficient, ΦHe = helium open porosity, ΦH_2O = water open porosity, Φ_c = closed porosity, Φ_t = total porosity, and S.I. = saturation index (italic differentiates standard deviations and arithmetic averages from the rest of the data).

Sample	Age	Function	ρ_R	ρ_B	ρ_S	CI_w	ΦHe	ΦH_2O	Φ_c	Φ_t	S.I.
			(g/cm^3)	(g/cm^3)	(g/cm^3)	(%)	(%)	(%)	(%)	(%)	(%)
SS 56	Romanesque (XI–XII Cent. AD)	Ashlar bedding	2.61	1.55	2.79	25.08	40.56	38.91	6.99	47.55	95.93
SS 57		Ashlar bedding	2.56	1.67	2.81	18.72	34.82	31.27	9.55	44.37	89.80
SS 58		Ashlar bedding	2.58	1.56	2.78	24.28	39.61	37.82	7.69	47.31	95.47
SS 59		Ashlar bedding	2.65	1.75	2.75	16.09	33.74	28.25	3.89	37.63	83.71
SS 94		Curtain wall filling	2.52	1.81	2.71	13.45	28.19	24.37	7.50	35.70	86.43
SS 95		Curtain wall filling	2.62	1.84	2.73	15.32	29.70	28.24	4.14	33.84	95.11
	Arithmetic average		*2.59*	*1.70*	*2.76*	*18.82*	*34.44*	*31.48*	*6.63*	*41.07*	*91.08*
	Standard deviation		*0.05*	*0.13*	*0.04*	*4.85*	*5.03*	*5.78*	*2.20*	*6.08*	*5.23*
SS 100	Roman (II–IV Cent. AD)	Ashlar bedding	2.57	1.53	2.78	22.78	40.33	34.93	8,12	48.45	86.62
SS 103		Ashlar bedding	2.54	1.69	2.65	18.49	33.59	31.24	4.26	37.85	93.02
SS 105		Ashlar bedding	2.47	1.47	2.64	25.64	40.55	37.67	6.68	47.23	92.90
SS 114		Ashlar bedding	2.60	1.67	2.73	18.66	35.68	31.19	4.92	40.60	87.44
SS 98		Curtain wall filling	2.51	1.68	2.73	17.41	33.17	29.23	8.88	42.05	88.10
SS 108		Curtain wall filling	2.61	1.64	2.75	20.49	37.32	33.54	5.26	42.59	89.87
	Arithmetic average		*2.55*	*1.61*	*2.71*	*20.58*	*36.77*	*32.97*	*6.36*	*43.13*	*89.66*
	Standard deviation		*0.05*	*0.09*	*0.06*	*3.12*	*3.21*	*3.05*	*1.86*	*4.02*	*2.77*

Table 7. Mechanical analysis of mortars. I_{S50} = point load strength index, R_c = compressive strength, and R_t = tensile strength (italic differentiates standard deviations and arithmetic averages from the rest of the data).

Sample	Mortar Age	Function	I_{S50} (MPa)	R_c (MPa)	R_t (MPa)
SS 56	Romanesque (XI–XII Cent. AD)	Ashlar bedding	0.94	13.10	1.17
SS 57		Ashlar bedding	0.95	13.36	1.19
SS 58		Ashlar bedding	0.70	9.82	0.88
SS 59		Ashlar bedding	0.81	11.35	1.01
SS 94		Curtain wall filling	0.76	10.69	0.95
SS 95		Curtain wall filling	0.48	6.75	0.60
	Arithmetic average		*0.77*	*10.84*	*0.97*
	Standard deviation		*0.17*	*2.43*	*0.22*
SS 100	Roman (II–IV Cent. AD)	Ashlar bedding	0.58	8.17	0.73
SS 103		Ashlar bedding	0.65	9.08	0.81
SS 105		Ashlar bedding	0.89	12.41	1.11
SS 114		Ashlar bedding	0.66	9.27	0.83
SS 98		Curtain wall filling	0.50	7.06	0.63
SS 108		Curtain wall filling	0.67	9.32	0.83
	Arithmetic average		*0.66*	*9.22*	*0.82*
	Standard deviation		*0.13*	*1.79*	*0.16*

4. Conclusions

The several analyses carried out in this investigation allow to understand the technology production of mortars in a time interval of 1000 years from Roman to Middle Ages, in order to find a match with the statements reported in the literature. Contrary to what was expected, the Romanesque mortars have higher mechanical qualities that allow them to have better performance on buildings. A greater pozzolanic activity distinguishes the Romanesque mortars from the Roman ones, probably describing in the latter the use of a weakly hydraulic micritic limestone outcropping a few hundred meters from the building. The use of different limestones is also evidenced by the presence of two different mortars placed in contact, which showed a different content of silicon and aluminium. In the production of mortars, only local limestone and sand aggregate were used. The use of obsidian is absent. This was found in the mortars of buildings relative to the same historical period identified in the nearby Roman city of Nora, in the castles of central Sardinia and in the buildings of the archaeological area of Tharros [32]. Physical analyses and particle-size distribution point out similar characteristics in between the two groups. In diffraction, the Roman mortars showed a whole series of sulphate alteration phases deriving from an external sulphate attack, while the composition of Medieval mortars was substantially uniform without any kind of sulphation. In thin section, both Roman and Romanesque mortars showed the presence of lumps derived from not uniform temperature in the lime kiln and insufficient mixing of the dough. In addition, in Roman mortars, the presence of ghosts lumps indicates inadequate firing in the kiln. These inclusions are normally frequent in ancient mortars because of the firing temperature and oxidant conditions difficult to control on kilns, depending on the technologies available at the time.

It can be concluded that the research, in this case study, highlights an overall better quality of medieval mortars compared to Roman ones, contrary to what is indicated in the other literature case study.

Funding: P.O.R. Sardegna F.S.E.—Operational Programme of the Autonomous Region of Sardinia, European Social Fund 2014–2020—Axis III Education and training, Thematic goal 10, Investment Priority 10ii), Specific goal 10.5.

Institutional Review Board Statement: Not applicable.

Informed Consent Statement: Not applicable.

Data Availability Statement: Not applicable.

Acknowledgments: Fabio Sitzia gratefully acknowledges Sardinian Regional Government for the financial support of his PhD scholarship.

Conflicts of Interest: The authors declare no conflict of interest.

References

1. Cagnana, A. *Archeologia dei Materiali da Costruzione*; SAP-Socirtà Archeologica S.R.L.: Mantova, Italy, 2000.
2. Wetmore, M.N.; Vitruvius, M.H.M. *Vitruvius: The Ten Books on Architecture, Class*; Dover: Malvern, UK, 1916. [CrossRef]
3. Bertonha, J.F. Em nome de Roma. In *História Questões Debates*; UFPR: London, UK, 2010. [CrossRef]
4. Furlan, V.; Bissegger, P. *Les Mortiers Anciens: Historie et Essais D'analyse Scientifiquesancient Mortars: History and Approach to Scientific Examination, Zeitschrift FÂ¸r Schweizerische Archâeologie Und Kunstgeschichte = Rev*; Suisse d'art d'archaeologie: Zurich, Switzerland, 1975.
5. Artioli, G.; Secco, M.; Addis, A. The vitruvian legacy: Mortars and binders before and after the Roman world. *Eur. Mineral. Union Notes Mineral.* **2019**. [CrossRef]
6. Manieri, G.E. *Metodo e Tecniche del Restauro Architettonico*; Carocci: Rome, Italy, 2010.
7. Amoroso, G. *Trattato di Scienza Della Conservazione dei Monumenti*; Alinea: Firenze, Italy, 2002.
8. Sitzia, F.; Beltrame, M.; Stefano, C.; Lisci, C.; Miguel, C.; Mirao, J. Ancient restoration and production technologies of Roman mortars from monuments placed in hydrogeological risk areas: A case study. *Archaeol. Anthropol. Sci.* **2020**, *12*, 147. [CrossRef]
9. Vola, G.; Gotti, E.; Brandon, C.; Oleson, J.P.; Hohlfelder, R.L. Chemical, mineralogical and petrographic characterization of Roman ancient hydraulic concretes cores from Santa Liberata, Italy and Caesarea Palestinae, Israel. *Period. Mineral.* **2011**, *80*, 317–338. [CrossRef]
10. Salvi, D. Cagliari: San Saturnino, le fasi altomedievali. In *Ai Confini dell'Impero: Storia, Arte e Archeologia della Sardegna Bizantina*; Corrias, P., Cosentino, S., Eds.; M & T, Cagliari: Cagliari, Italy, 2002; pp. 225–229.
11. Coroneo, R. *Architettura Romanica Dalla Metà del Mille al Primo '300*; Ilisso: Nuoro, Italy, 1993.
12. Letezia, E. *Il Complesso Martiriale di San Saturno*; Christ: Torino, Italy, 1992; pp. 55–81.
13. Boscolo, A. *L'Abbazia di San Vittore*; Pisa e la Sardegna: Padova, Italy, 1988.
14. Coroneo, R.; Serra, R. *Sardegna Preromanica e Romanica*; Milano, Jaca Book: Milan, Italy, 2004.
15. Ermini, L.P. Ricerche nel complesso di S. saturno a Cagliari. *Rend. Della Pontif. Accad. Rom. d'Archeol.* **1984**, *84*, 111–128.
16. Kirova, K.T. *La Basilica di S. Saturnino in Cagliari. la Sua Storia e i Suoi Restauri*; Minipress: Cagliari, Italy, 1979.
17. Delogu, R. *L'architettura del Medioevo in Sardegna*; La libreri: Rome, Italy, 1954.
18. Coroneo, R. La basilica di San Saturnino a Cagliari nel quadro dell'architettura mediterranea del VI secolo. *San Saturnino Patrono Della Città Cagliari* **2004**, *17*, 55–83.
19. Columbu, S.; Antonelli, F.; Sitzia, F. Origin of Roman worked stones from St. Saturno christian Basilica (south Sardinia, Italy). *Mediterr. Archaeol. Archaeom.* **2018**, *18*, 17–36. [CrossRef]
20. Grillo, S.M.; Prochaska, W. The marble inventory of the early christian Basilica San Saturnino/Cagliari-Sardinia). In *CHNT16 Urban Archaeol*; Boerner, W., Ed.; Prospect: Wien, Austria, 2014.
21. Ortega, L.A.; Zuluaga, M.C.; Alonso-Olazabal, A.; Insausti, M.; Ibáñez, A. Geochemical characterization of archaeological lime mortars: Provenance inputs. *Archaeometry* **2008**, *50*, 387–408. [CrossRef]
22. Miriello, D.; Bloise, A.; Crisci, G.M.; Apollaro, C.; la Marca, A. Characterisation of archaeological mortars and plasters from kyme (Turkey). *J. Archaeol. Sci.* **2011**, *38*, 794–804. [CrossRef]
23. Silva, D.A.; Wenk, H.R.; Monteiro, P.J.M. Comparative investigation of mortars from Roman Colosseum and cistern. *Thermochim. Acta* **2005**, *438*, 35–40. [CrossRef]
24. Riccardi, M.P.; Duminuco, P.; Tomasi, C.; Ferloni, P. Thermal, microscopic and X-ray diffraction studies on some ancient mortars. *Thermochim. Acta* **1998**, *321*, 207–214. [CrossRef]
25. Montoya, C.; Lanas, J.; Arandigoyen, M.; Casado, P.J.G.; Alvarez, J.I. Mineralogical, chemical and thermal characterisations of ancient mortars of the church of Santa María de Irache Monastery (Navarra, Spain). *Mater. Struct. Constr.* **2004**, *37*, 433–439. [CrossRef]
26. Moropoulou, A.; Bakolas, A.; Bisbikou, K. Investigation of the technology of historic mortars. *J. Cult. Herit.* **2000**, *1*, 45–58. [CrossRef]
27. Crisci, G.M.; Franzini, M.; Lezzerini, M.; Mannoni, M.; Riccardi, M.P. Ancient mortars and their binders. *Period. Mineral.* **2004**, *73*, 259–268.
28. Krumbein, W.C. Measurement and geological significance of shape and roundness of sedimentary particles. *SEPM J. Sediment. Res.* **1941**, *11*. [CrossRef]
29. Palmström, A. RMi–A Rock Mass Characterization System for Rock Engineering Purposes. Ph.D. Thesis, University of Oslo, Oslo, Norway, 1995.
30. Pecchioni, E.; Frattini, F.; Cantisani, E. *Le Malte Antiche e Moderne tra Tradizione ed Innovazione*; Patron: Bologna, Italy, 2018.
31. Regione Autonoma Della Sardegna. *Indagine Amministrativa e Tecnico-Scientifica Sugli Interventi Eseguiti nel Litorale del Poetto-Relazione Conclusiva*; Regione Autonoma Della Sardegna: Cagliari, Italy, 2006.

32. Sitzia, F. *Degradation Monitoring and Conservation of Sardinia Monumental Heritage by Geochemical, Petrographic, Physical and Micro-Photogrammetric Characterization of Stone Surfaces*; University of Cagliari: Cagliari, Italy, 2019.
33. Sitzia, F.; Lisci, C.; Mirão, J. Accelerate ageing on building stone materials by simulating daily, seasonal thermo-hygrometric conditions and solar radiation of Csa Mediterranean climate. *Constr. Build. Mater.* **2021**, *266*, 121009. [CrossRef]
34. Columbu, S.; Marchi, M.; Martorelli, R.; Palomba, M.; Pinna, F.; Sitzia, F.; Tanzini, L.; Virdis, A. *Architettura Romanica e Territorio*; CUEC: Cagliari, Italy, 2018.
35. Previato, C.N. *Le Cave di Pietra Della Città Antica*; Quasar: Rome, Italy, 2016.
36. Stefano, C.; Garau, A.M.; Lugliè, C. Geochemical characterisation of pozzolanic obsidian glasses used in the ancient mortars of Nora Roman theatre (Sardinia, Italy): Provenance of raw materials and historical–archaeological implications. *Archaeol. Anthropol. Sci.* **2018**, *11*, 2121–2150. [CrossRef]
37. Garau, A.M. *Le Pietre e le Malte del Teatro di Nora (Sardegna SW)*; Università degli Studi di Cagliari: Cagliari, Italy, 2005.
38. Stepkowska, E.T.; Pérez-Rodríguez, J.L.; Sayagués, M.J.; Martínez-Blanes, J.M. Calcite, vaterite and aragonite forming on cement hydration from liquid and gaseous phase. *J. Therm. Anal. Calorim.* **2003**, *73*, 247–269. [CrossRef]
39. Signorelli, S.; Peroni, C.; Camaiti, M.; Fratini, F. The presence of vaterite in bonding mortars of marble inlays from Florence Cathedral. *Mineral. Mag.* **1996**, *60*, 663–665. [CrossRef]
40. De Leeuw, N.H.; Parker, S.C. Surface structure and morphology of calcium carbonate polymorphs calcite, aragonite, and vaterite: An atomistic approach. *J. Phys. Chem. B* **1998**, *102*, 2914–2922. [CrossRef]
41. Cole, W.F.; Kroone, B. Carbon dioxide in hydrated portland cement. *ACI J. Proc.* **1960**, *65*, 6. [CrossRef]
42. Ikumi, T.; Cavalaro, S.H.P.; Segura, I. The role of porosity in external sulphate attack. *Cem. Concr. Compos.* **2019**, *97*, 1–12. [CrossRef]
43. Hajilar, S. *Nano-Scale Investigation of Mechanical Characteristics of Main Phases of Hydrated Cement Paste*; University of Massachussets Amherst: Amherst, MA, USA, 2015.
44. Columbu, S.; Sitzia, F.; Ennas, G. The ancient pozzolanic mortars and concretes of heliocaminus baths in Hadrian's Villa (Tivoli, Italy). *Archaeol. Anthropol. Sci.* **2017**, *9*, 523–553. [CrossRef]
45. Varga, V. The structure of kaolinite and metakaolinite. Epitoanyag. *J. Silic. Based Compos. Mater.* **2007**, *59*, 6–9. [CrossRef]
46. Columbu, S.; Gioncada, A.; Lezzerini, M.; Sitzia, F. Mineralogical-chemical alteration and origin of ignimbritic stones used in the Old cathedral of nostra signora di castro (Sardinia, Italy). *Stud. Conserv.* **2019**, *64*, 397–422. [CrossRef]
47. Wentworth, C.K. A scale of grade and class terms for clastic sediments. *J. Geol.* **1922**, *30*, 377–392. [CrossRef]